Biophysical Journal, Volume *114*

Supplemental Information

Mechanisms of Plastic Deformation in Collagen Networks Induced by Cellular Forces

Ehsan Ban, J. Matthew Franklin, Sungmin Nam, Lucas R. Smith, Hailong Wang, Rebecca G. Wells, Ovijit Chaudhuri, Jan T. Liphardt, and Vivek B. Shenoy

SUPPORTING METHODS

Acinar culture

MCF10AT acini were cultured and extracted as previously described (1, 2). Briefly, MCF10AT cells were seeded at a density of about 4,000 cells/mL in a 2:1 mixture of growth-factor-reduced Matrigel (Corning, Corning, NY):MCF10A growth media (1). Media was exchanged every two days. MCF10AT cells behave similarly to the MCF10A cells because they are the Ras transformation of the MCF10A cells. The media, however, must be changed more frequently when using MCF10AT than would be necessary for experiments using MCF10A because the cell-division rate of MCF10AT cells is higher. Acini were extracted from Matrigel after eight days using ice-cold ten mM Tris buffer/5 mM EDTA. Acini were washed three times with a five-minute incubation period on ice with gentle mixing and were then spun down at 100 x g after washes. Acini were resuspended in F12/DMEM with 20% (vol/vol) horse serum, spun once again, and finally resuspended in MCF10A growth media.

Collagen staining for the acini experiments

EGFP from the pET E. coli expression vector containing 6xhis-CNA35-EGFP (2) was replaced with the SNAP-tag® (NEB). As previously described, protein was purified from a 1 L culture of BL21(DE3) pLysE cells transformed with the CNA35-SNAP® (2). The purified protein was stained using SNAP-Cell® 647-SiR fluorescent substrate according to the manufacturer's protocol. Collagen gels containing acini were stained with 50 µg of CNA35-SNAP-647SiR for 30 minutes in a cell culture incubator at 37°C. Gels were washed twice with warm MCF10A media and transferred to the microscope for imaging.

Acinus time-lapse imaging

Acini were imaged using a Zeiss LSM700 inverted microscope using an EC Plan-Neofluar 5x NA0.16 objectives. During acinar contraction, images were recorded every 30 minutes with the sequential acquisition of the 555 nm (1% power) and 639 nm (2% power) lasers. After the addition of the inhibitor cocktail, images were taken every 8 minutes. A live-cell imaging box was used to maintain a temperature of 37°C and 6% CO2. Tiled images were stitched using software supplied by Zeiss.

Measurement of the in-plane gel deformation and stretch fields

For measuring substrate displacement, 1 µm Nile-red (535/575) fluorescent beads (Life Technologies, Carlsbad, CA) were added at 2000X dilution from a 2% (wt/vol) stock. In-Plane gel deformation was measured by projecting a 30-µm thick volume centered at the surface of the gel and using particle image velocimetry (3) to generate displacement vector fields, $\boldsymbol{u}$ (Fig. S1a). For a material particle moving from position $\boldsymbol{X}$ to position $\boldsymbol{x}$, $\boldsymbol{u}$ was evaluated as $\boldsymbol{x} - \boldsymbol{X}$. The displacement field was then used to numerically calculate the deformation gradient tensor $\mathbf{F} = \nabla_{\boldsymbol{X}}\boldsymbol{x}$, in index notation: $F_{ij} = \partial x_i / \partial X_j$. In the case where $\boldsymbol{X}$ corresponds to the initial position of a point and $\boldsymbol{x}$ corresponds to its position at time t, the resulting deformation gradient is $\mathbf{F}(t)$, which appears in Eq. (1) of the main text. The deformation gradient was then used to calculate the stretch tensor as $\mathbf{U} =$

$(\mathbf{F}^{\mathrm{T}}\mathbf{F})^{1/2}$. Principal stretches are the eigenvalues of $\mathbf{U}$ (4). Apparent Poisson's ratio (5) was calculated as $(1-\lambda')/(\lambda-1)$, where λ' and λ denote stretch ratios in the transverse and axial directions.

Collagen gel formulation for the fibroblast experiments

Solubilized rat tail collagen (Sigma-Aldrich, Saint Louis, MO) was diluted to a final concentration of 1.5 mg/mL with 10X PBS and deionized water and was neutralized to pH 7.0 with NaOH. The collagen solution was pre-incubated at 4°C for an hour before being plated in the 14-mm glass bottom portion of a 35-mm dish (MatTek, Ashland, MA). The plate was then sealed with Parafilm (Bemis NA, Neenah, WI) and incubated at 37°C overnight.

Second harmonic generation imaging

Fibrillar collagen was visualized by second harmonic generation (SHG) imaging with a Coherent Chameleon Ultra II Ti: Sapphire laser tuned to 800 nm and a Leica SP5 upright confocal/multiphoton system with a 20x (1.0 NA) water immersion lens. Non-descanned detectors were used to capture the SHG signal as well as images of cellular auto-fluorescence. Z-stacks were collected over a range 10 μm above and below the maximum intensity in the tract region. To quantify the degree of bridging between spheroids, a region of interest was specified that spanned the total length between the spheroids and was as wide as the spheroids. The average projection was taken and the average intensity of the SHG channel was quantified. The anisotropy of the intensity of SHG was then used to evaluate fiber alignment (6).

Mikado fiber network model

Fibers with random positions and orientations were placed in a two-dimensional rectangular region, and crosslinks were formed between intersecting fibers. Individual fibers were modeled using elastic beams with circular cross-sections of diameters 100 nm, elastic moduli 6 MPa, and Poisson's ratios of 0.3. The finite element simulations were performed using beams with a reduced integration (7) scheme and the Riks analysis method (8). Displacement-controlled tests were conducted by prescribing the nodal displacement at the network boundaries in the direction of loading while allowing free network contraction in the other directions. Transient crosslinks were updated at each time step. We used k_0 =0.01 h^{-1} and a threshold length of 8 μm to determine the rate of crosslink formation. The finite element model was updated after the addition or removal of elements.

Collagen gel preparation for shear rheology experiments

Solutions of collagen type I (Corning, Corning, NY) were prepared on ice by neutralizing with 1N NaOH and 10× Dulbecco's modified Eagle's medium (DMEM) and diluting with 1× DMEM to a designated concentration. The collagen solution was immediately deposited on the rheometer plates before experiments and heated to 37°C.

Diluted lattice network model of fiber level plasticity

A network of fibers was constructed by connecting the first and second nearest neighbors in a body-centered cubic lattice. A portion of the lattice edges was then randomly removed to produce a diluted network of desired collagen volumetric fraction. The fibers passing through a lattice point were detached from each other to produce networks with local connectivities matching collagen gels. Fibers were modeled using Timoshenko beams flexible in stretching, bending, twisting and transverse shear. Beams with hybrid formulation (4), reduced integration (7), and circular cross-sections of diameter 100 nm were used in the finite element model. The model was solved using the finite element package Abaqus (9). Implicit static and dynamic simulations were performed, ensuring that the kinetic energy is orders of magnitude smaller than elastic energy in all cases.

Generation of the Voronoi network

First, random points in a three-dimensional domain were chosen as seed points. The Voronoi diagram corresponding to these seed points was then generated using MATLAB (MathWorks, Natick, MA). Beam elements were then considered along the edges of the Voronoi diagram to model fibers. To perform mechanical tests, we extracted a cubic sample from the constructed network.

SUPPORTING FIGURES

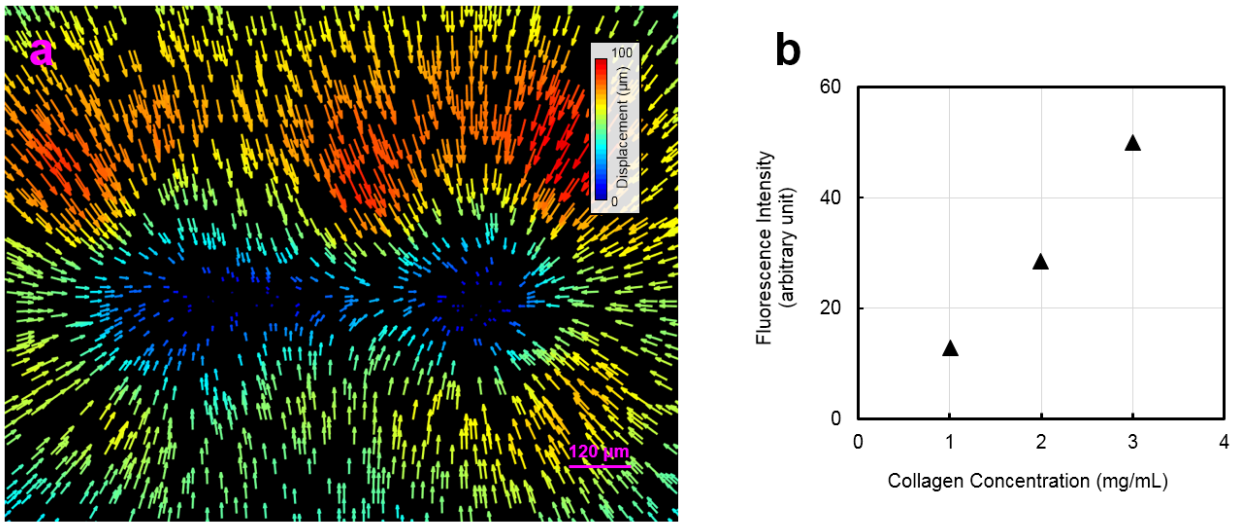

FIGURE S1 (a) Example of a displacement field measured by tracking fluorescent beads around an isolated pair of interacting acini. (b) Control tests show the dependence of fluorescence intensity on collagen concentration.

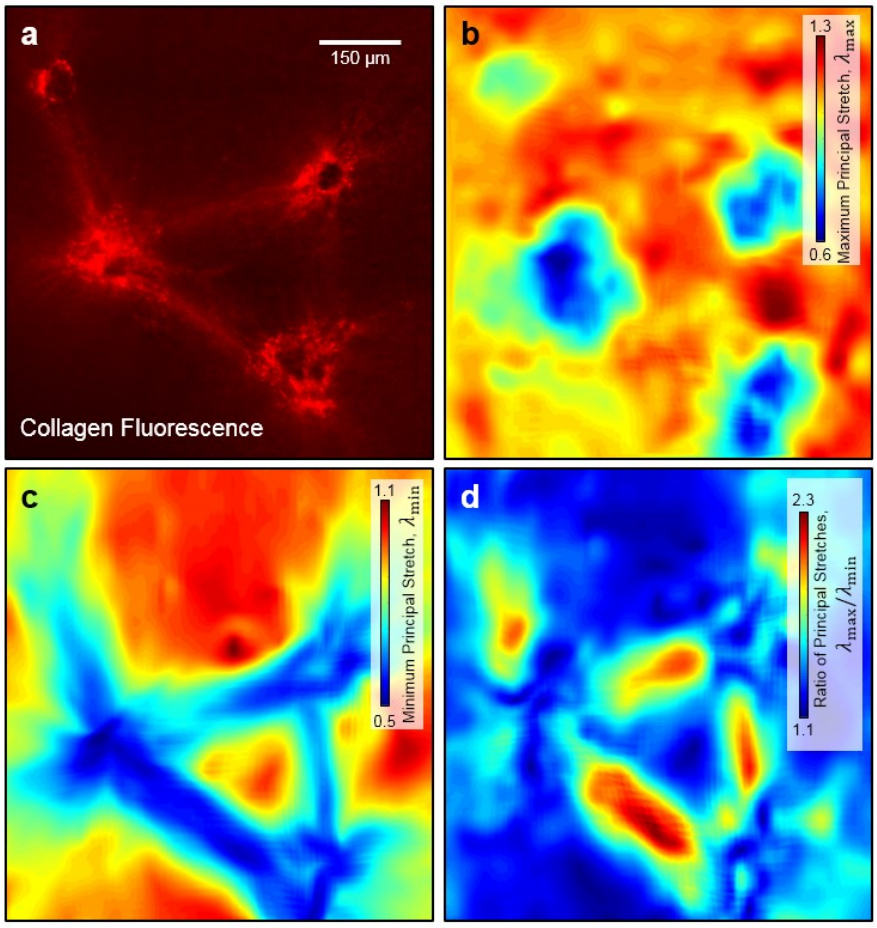

FIGURE S2 Fluorescence intensity and principal stretches in the multiple acini experiments. (a) Fluorescence from collagen labeling proteins. (b and c) the maximum and minimum principal stretches. (d) Large ratio of principal stretches in a system of four contractile acini along the tracts, signifying substantial Poisson effects. All plots correspond to the onset of contractility inhibition.

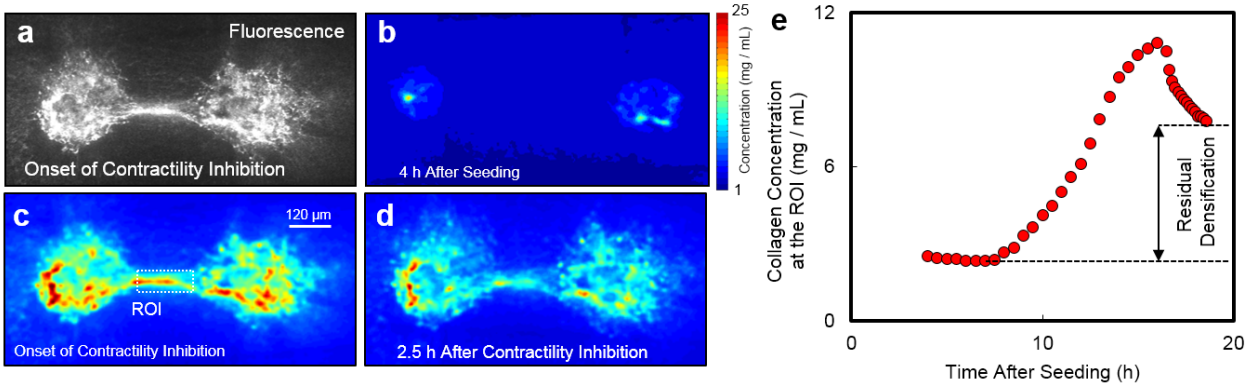

FIGURE S3 Plasticity of a collagen tract formed by a pair of contractile acini. (a) Fluorescence from collagen binding markers at the onset of contractility inhibition. Collagen density (b) 4 h after seeding the acini, (c) at the onset of inhibiting contractility (17 h after seeding), and (d) 2.5 h after inhibiting contractility. (e) Variation of local collagen density at the region of interest (ROI) marked in panel (c).

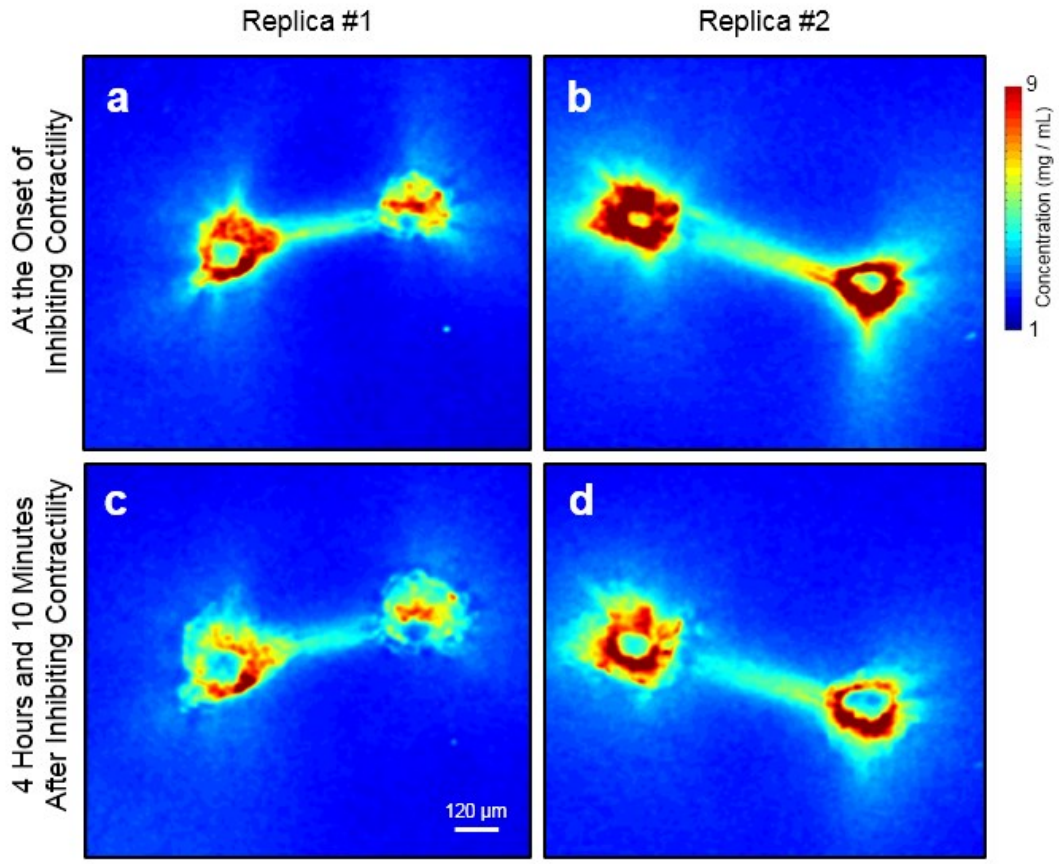

FIGURE S4 Inhibition of the formation of new crosslinks by LOX using β-aminopropionitrile (BAPN) added after seeding the acini did not influence the plastic effects. (a and b) The concentration of collagen measured using fluorescence in experimental replicas #1 and #2 at the onset of inhibition of contractility. (c and d) The same experiments 4 hours and 10 minutes after contractility was inhibited.

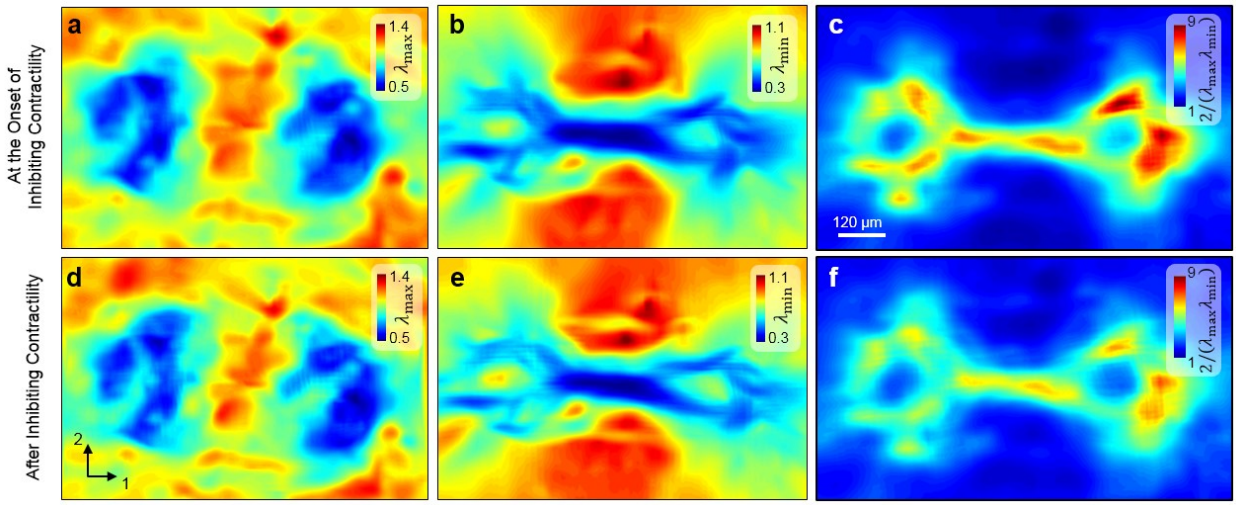

FIGURE S5 Stretch maps in experiments with a pair of contractile acini. $\lambda_{\max}$ and $\lambda_{\min}$ denote the stretch ratios in the directions parallel and perpendicular to the axis of the collagen tract respectively. (a) $\lambda_{\max}$, (b) $\lambda_{\min}$ and (c) density estimate using displacement field at the onset of inhibiting contractility. (d) $\lambda_{\max}$, (e) $\lambda_{\min}$ and (f) density estimate using displacement fields after inhibiting cellular contraction.

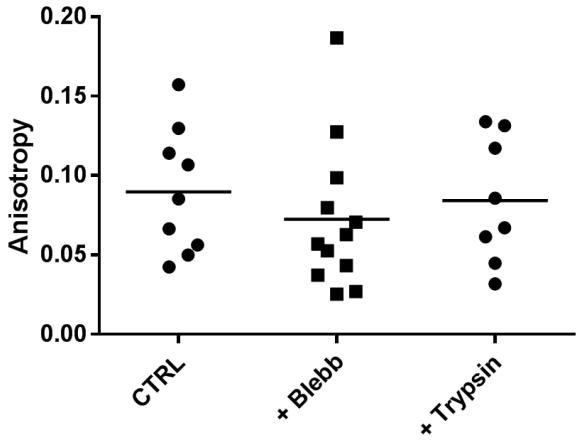

FIGURE S6 Anisotropy calculated using SHG in the fibroblast experiments. The three sets of points correspond to the control and the cases where contractility was inhibited using blebbistatin and trypsin.

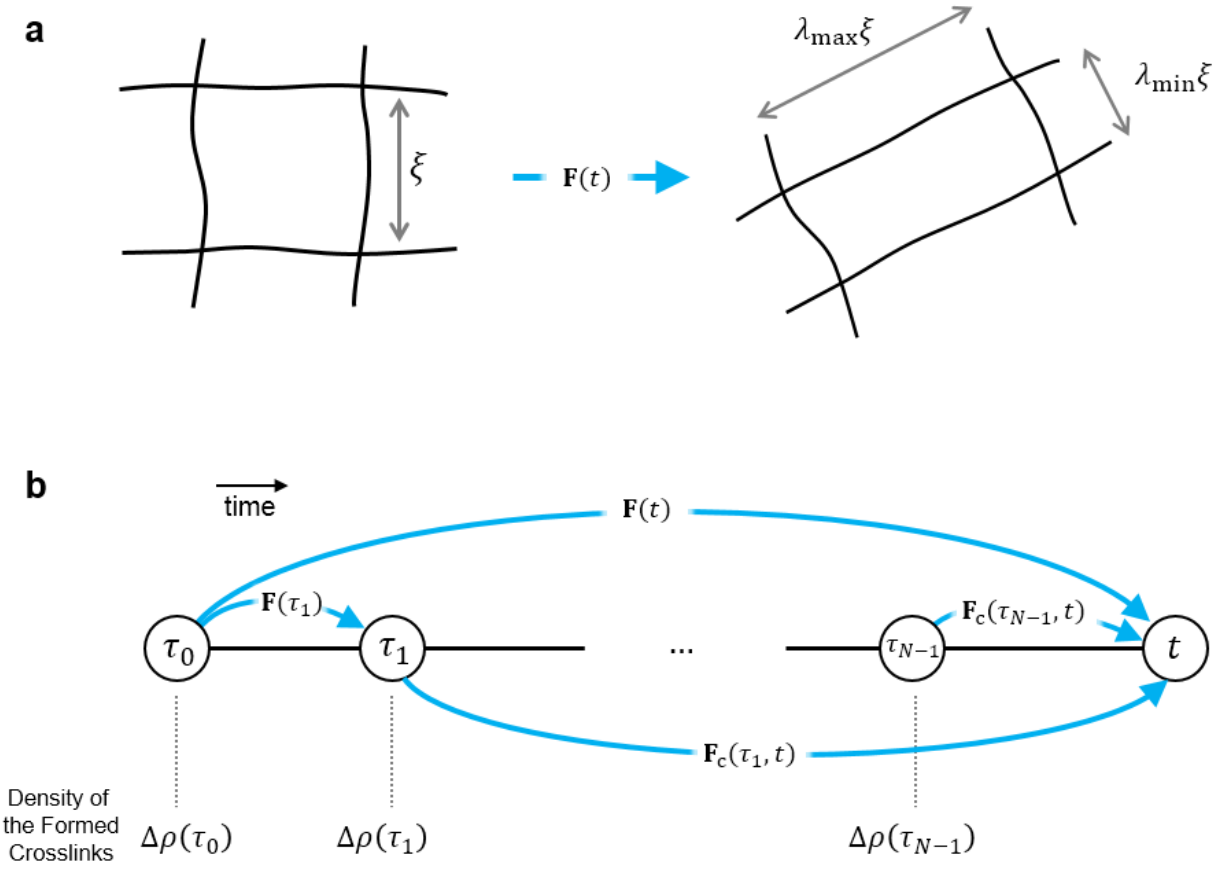

FIGURE S7 Modeling crosslinking formation and breaking in the coarse-grained plastic constitutive model. (a) Approximate network mesh size, ξ, before and after network stretch. (b) Timesteps: 0, τ_1 to τ_{N-1} and t. $\Delta\rho(\tau_i)$ is the density of crosslinks formed at the time point τ_i. The contribution of crosslinks formed at time τ_i to strain energy at time t is determined using the relative deformation gradient between instants τ_i and t, $\mathbf{F}_c(\tau_i, t)$. $\mathbf{F}_c(\tau_i, t)$ may be evaluated as $\mathbf{F}(t)\mathbf{F}(\tau_i)^{-1}$.

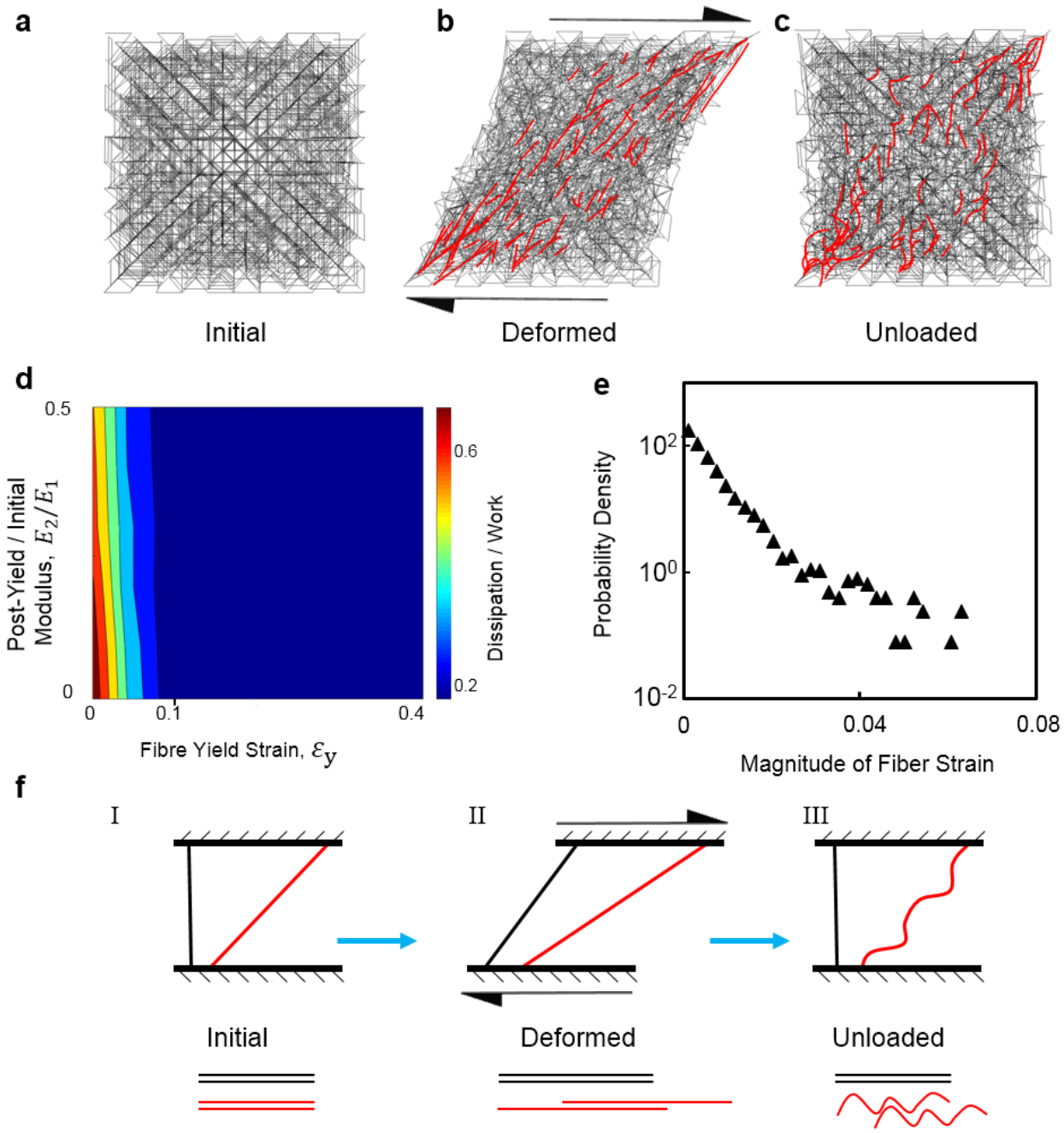

FIGURE S8 Microstructural network plasticity by permanent elongation of fibers at small to moderate levels of strain. (a–c) Network snapshots show the permanent elongation of fibers along the maximum principal stretch direction and their subsequent buckling when the network is unloaded. (d) Normalized energy dissipation as a function of fiber yield strain and normalized hardening modulus, E_2. (e) Nonuniform distribution of the magnitude of axial strain in fibers in the random lattice based network model with plastically elongated fibers (at γ=0.4) (f) Schematic of the deformation unloading mechanism in networks with plastic fibers in the (I) initial, (II) deformed, and (III) unloaded states. Relative sliding of protofibrils results in the permanent elongation of fibers.

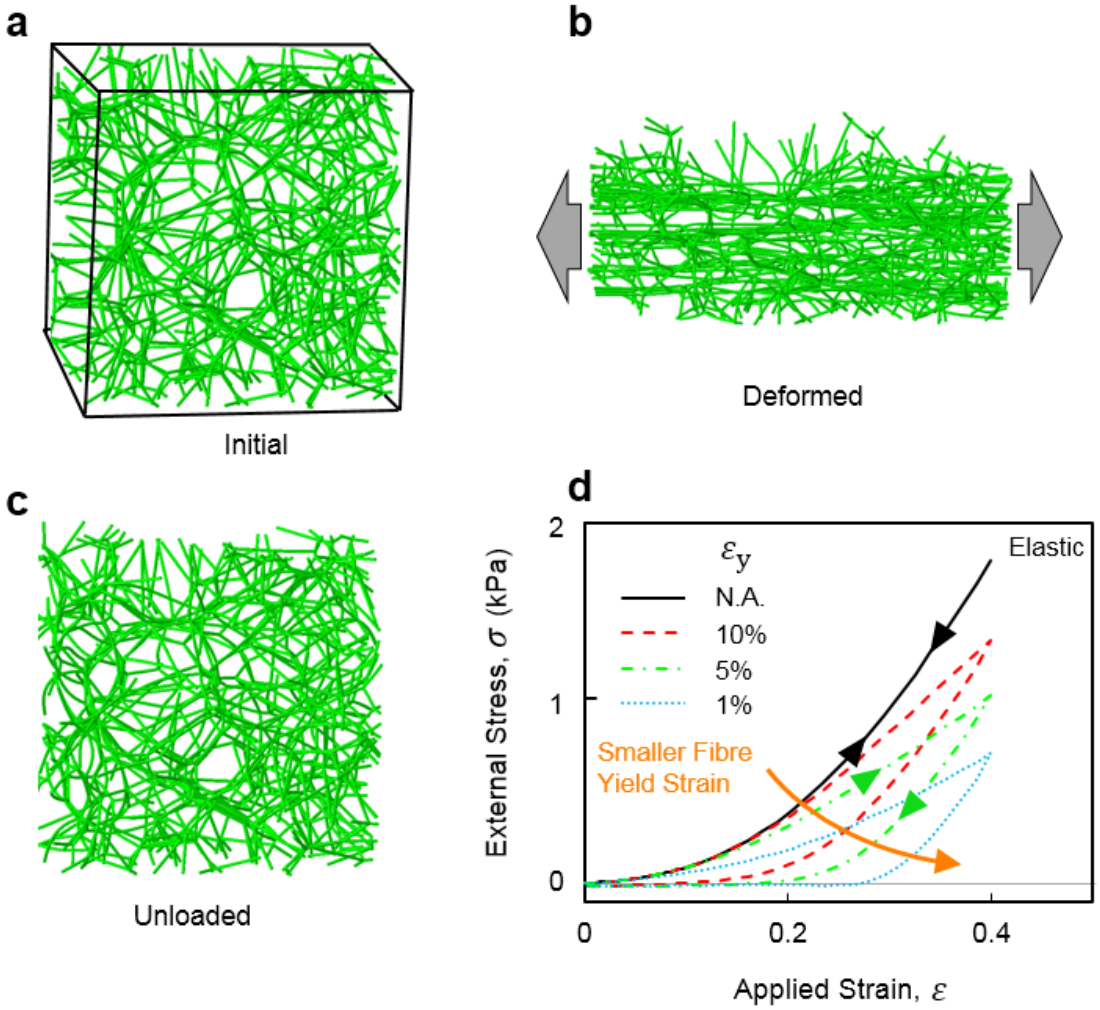

FIGURE S9 Absence of macroscopic plastic strains after removing external loads during uniaxial stretch of a Voronoi network up to 40% strain. (a–c) Snapshots of the network in the (a) initial, (b) deformed, and (c) unloaded states. (d) Stress-strain curves for a network of (solid black) elastic fibers and plastic fibers with yield strains, ε_y, of (dashed red) 10%, (dashed-dotted green) 5% and (dotted blue) 1%. Smaller fiber yield strain leads to larger plastic dissipation in the network. However, when external forces are removed negligible macroscopic strains remain in all cases, signifying the absence of plastic strains at the network scale at small to moderate applied amplitudes of strain.

TABLE S1 Crosslink formation and dissociation parameters used in the coarse-grained constitutive model. The model parameters were estimated to reproduce the viscoplastic response of collagen gels in creep and recovery shear rheology tests (Fig. 3a of the main text).

Parameter	Value
$\bar{k}_{\mathrm{off}}^{0}$	7.0×10^{-3} s^{-1}
$\bar{k}_{\mathrm{on}}^{0}$	5.0 s^{-1}
$\bar{\varepsilon}_{0}$	1.0
$\bar{\lambda}_{0}$	3.2×10^{-2}
$\bar{\lambda}_{\mathrm{eq}}$	1.0
α	3.0×10^{-3}
$\bar{k}'^{0}_{\mathrm{off}}$	5.5×10^{-1} s^{-1}
$\bar{k}'^{0}_{\mathrm{on}}$	5.0×10^{1} s^{-1}
$\bar{\varepsilon}'_{0}$	8.9
$\bar{\lambda}'_{0}$	8.6
$\bar{\lambda}'_{\mathrm{eq}}$	7.3×10^{-1}

SUPPORTING REFERENCES

1. Debnath, J., S.K. Muthuswamy, and J.S. Brugge. 2003. Morphogenesis and oncogenesis of MCF-10A mammary epithelial acini grown in three-dimensional basement membrane cultures. Methods. 30: 256–268.

2. Shi, Q., R.P. Ghosh, H. Engelke, C.H. Rycroft, L. Cassereau, J.A. Sethian, V.M. Weaver, and J.T. Liphardt. 2014. Rapid disorganization of mechanically interacting systems of mammary acini. Proc. Natl. Acad. Sci. 111: 658–663.

3. Thielicke, W., and E. Stamhuis. 2014. PIVlab – Towards User-friendly, Affordable and Accurate Digital Particle Image Velocimetry in MATLAB. J. Open Res. Softw. 2: e30.

4. Beatty, M.F., and D.O. Stalnaker. 1986. The Poisson Function of Finite Elasticity. J. Appl. Mech. 53: 807–813.

5. Boudaoud, A., A. Burian, D. Borowska-Wykręt, M. Uyttewaal, R. Wrzalik, D. Kwiatkowska, and O. Hamant. 2014. FibrilTool, an ImageJ plug-in to quantify fibrillar structures in raw microscopy images. Nat. Protoc. 9: 457–463.

6. Hughes, T.J.R. 1987. The Finite Element Method: Linear Static and Dynamic Finite Element Analysis. Prentice-Hall, Inc, Englewood Cliffs, NJ.

7. Riks, E. 1979. An incremental approach to the solution of snapping and buckling problems. Int. J. Solids Struct. 15: 529–551.

8. Bower, A.F. 2009. Applied Mechanics of Solids. CRC Press, Boca Raton, FL.

9. Hibbett, Karlsson, and Sorensen. 1998. ABAQUS/standard: User's Manual, Hibbitt, Karlsson & Sorensen, Providence, RI.